Rapid Communications

# Quantum spin Hall effect in monolayer and bilayer $TaIrTe_4$

Peng-Jie Guo, Xiao-Qin Lu, Wei Ji, Kai Liu,* and Zhong-Yi Lu†
*Department of Physics and Beijing Key Laboratory of Opto-electronic Functional Materials & Micro-nano Devices, Renmin University of China, Beijing 100872, China*

(Received 5 November 2019; revised 22 May 2020; accepted 25 June 2020; published 8 July 2020)

Generally, stacking two quantum spin Hall insulators gives rise to a trivial insulator. Here, based on first-principles electronic structure calculations, we confirm that monolayer $TaIrTe_4$ is a quantum spin Hall insulator and remarkably find that bilayer $TaIrTe_4$ is still a quantum spin Hall insulator. Theoretical analysis indicates that the covalentlike interlayer interaction in combination with the small band gap at the time-reversal invariant Γ point results in new band inversion in bilayer $TaIrTe_4$, namely, the emergence of quantum spin Hall phase. Meanwhile, a topological phase transition can be observed by increasing the interlayer distance in bilayer $TaIrTe_4$. Considering that bulk $TaIrTe_4$ is a type-II Weyl semimetal, layered $TaIrTe_4$ thus provides an ideal platform to realize different topological phases at different dimensions.

DOI: 10.1103/PhysRevB.102.041109

*Introduction*. Topological properties of real materials have attracted much attention both experimentally and theoretically in recent years. A quantum spin Hall (QSH) insulator, namely, a two-dimensional topological insulator, has a band gap in the bulk and the topologically protected metallic states at the edge [1,2]. Theoretically, the stacking of two QSH insulators together gives rise to a trivial insulator. Nevertheless, in real materials, a non-negligible, even strong interlayer interaction may exist for two stacked QSH insulators, which may lead to broadening of valence and conduction bands. As a result, one may ask: is it possible that stacking two quantum spin Hall insulators still gives rise to a QSH insulator in real materials? If so, this will provide a new platform for studying the QSH effect with more adjustable freedom. Due to the interlayer interaction, stacking two bilayer Bi(111) films still results in a QSH insulator [3–6]. So a natural idea is whether or not a weak van der Waals (vdW) interaction can lead to a similar result.

The interlayer interactions in vdW materials have given rise to many interesting physical phenomena and attracted intensive attention recently, for example, the layer-dependent ferromagnetism in $CrI_3$ [7]. Among various layered topological materials, tellurides have been intensively studied. Layered $WTe_2$ is a type-II Weyl semimetal in bulk form [8] while its monolayer is a QSH insulator with a direct band gap [9]. Bulk $TaIrTe_4$, sharing the same nonsymmorphic space group symmetry as $WTe_2$, was firstly proposed to be a type-II Weyl semimetal with the minimum four Weyl points under time-reversal symmetry constraint [10–13]. A later joint theory and experiment study suggested that bulk $TaIrTe_4$ has 12 Weyl points and a pair of node lines protected by a mirror symmetry [14]. Meanwhile, two studies indicated that monolayer $TaIrTe_4$ is a QSH insulator [15,16]. Considering that tellurides show abundant layer-dependent electronic structures [17,18], it is interesting to investigate the topological properties of $TaIrTe_4$ at the two-dimensional (2D) limit.

In this Rapid Communication, based on first-principles electronic structure calculations, we confirm that monolayer $TaIrTe_4$ is a quantum spin Hall insulator [15]. More interestingly, in contrast to the general perception that stacking two quantum spin Hall insulators would give rise to a trivial insulator, we exceptionally find that bilayer $TaIrTe_4$ is still a quantum spin Hall insulator. We have further explored the underlying physical mechanism theoretically.

*Method*. The electronic structures of ultrathin film $TaIrTe_4$ were studied with the projector augmented wave method [19,20] as implemented in the VASP package [21–23]. The Perdew-Burke-Ernzerhof-type exchange-correlation functional at the generalized gradient approximation level was adopted to describe the interaction between ionic core and valence electrons [24]. The kinetic energy cutoff of the plane-wave basis was set to 400 eV. The Gaussian smearing method with a width of 0.05 eV was utilized for the Fermi surface broadening. For the structural relaxation of bulk $TaIrTe_4$, the optB86b-vdW functional [25] was adopted to account for the interlayer interactions and an $18 \times 6 \times 6$ $k$-point mesh was used for the Brillouin zone (BZ) sampling. Both cell parameters and internal atomic positions were fully relaxed until the forces on all atoms were smaller than 0.01 eV/Å. The calculated lattice parameters of bulk $TaIrTe_4$ are in good agreement with the experimental values [26]. For the monolayer and bilayer calculations, the in-plane lattice constants were fixed to the relaxed bulk values, while the internal atomic positions were fully relaxed with an $18 \times 6 \times 1$ $k$-point mesh for the surface BZ sampling. A 20 Å vacuum layer was used to avoid the residual interaction between adjacent layers. The topological invariants and the edge states of monolayer and bilayer $TaIrTe_4$ were studied at the equilibrium structures by using the WannierTools package [27].

*Results*. Similar to type-II Weyl semimetal $WTe_2$, bulk $TaIrTe_4$ has a noncentrosymmetric crystal structure, adopting

*kliu@ruc.edu.cn
†zlu@ruc.edu.cn

 

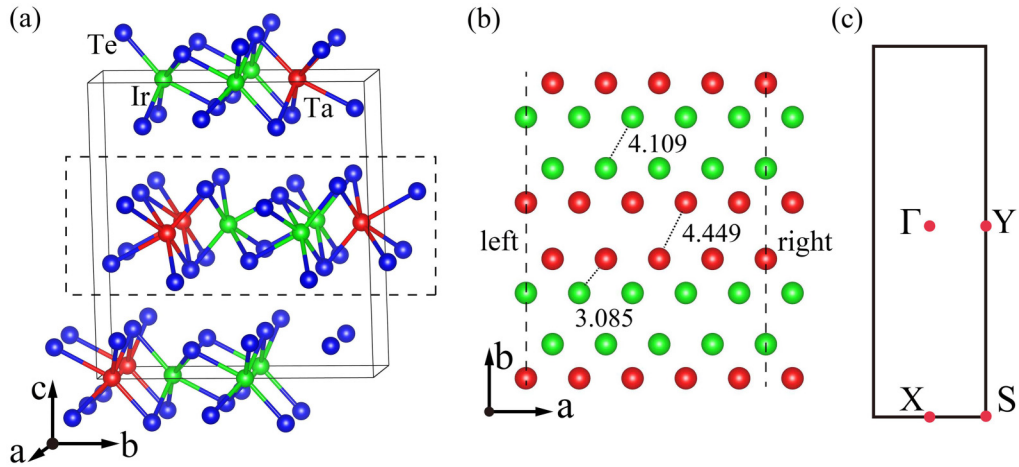


FIG. 1. (a) Crystal structure of bulk $TaIrTe_4$. The red, green, and blue balls denote Ta, Ir, and Te atoms, respectively. The dashed rectangle highlights the layered structure. (b) Top view of monolayer $TaIrTe_4$, where Te atoms are hidden for clarity. Several typical interatomic distances are labeled. The dashed lines with labels "left" and "right" denote two different terminations of thin-layer $TaIrTe_4$, respectively. (c) Surface Brillouin zone (BZ) of monolayer $TaIrTe_4$. The red dots represent the high-symmetry $k$ points.

a layered $1T'$ structure and $AB$ stacking, as shown in Fig. 1(a). Due to the structural distortion along the $b$ axis, Ta and Ir atoms form zigzag chains along the $a$ axis [Fig. 1(b)]. The space group symmetry of bulk $TaIrTe_4$ is $Pmn2_1$, and the corresponding four point-group symmetric operations are identity $E$, mirror reflection $M_x$, screw operation $\{C_{2z}|(1/2, 0, 1/2)\}$, and glide reflection $\{M_y|(1/2, 0, 1/2)\}$, respectively.

Due to its layered structure, one would like to know whether or not $TaIrTe_4$ can be exfoliated as many other 2D materials. We calculated the energy of $TaIrTe_4$ as a function of the interlayer distance. As shown in Fig. 2, the cleavage energy of $TaIrTe_4$ is 0.43 $J/m^2$, which is slightly larger than that of graphite (0.36 $J/m^2$) [28]. This indicates that an atomically thin film of $TaIrTe_4$ is likely obtained by mechanical exfoliation as graphene. In fact, an atomically thin film of $TaIrTe_4$ has been obtained by mechanical exfoliation [29].

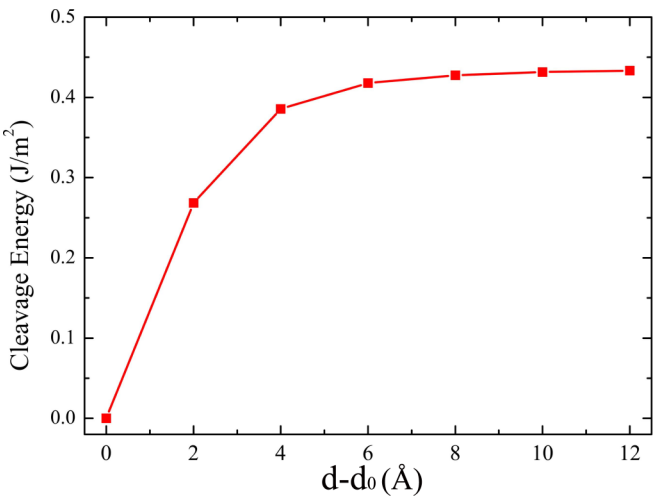


FIG. 2. Evolution of the total energy of bulk $TaIrTe_4$ with interlayer distance $d$. Here $d_0$ denotes the equilibrium interlayer distance.

To study the possible topological property of bilayer $TaIrTe_4$, we need to first clarify the electronic structure of monolayer $TaIrTe_4$. In comparison with bulk $TaIrTe_4$, the space group of monolayer $TaIrTe_4$ changes to $P12_1/m1$ with additional inversion symmetry, but losing nonsymmorphic symmetry operation of the fractional translation along the $c$ axis. The corresponding surface Brillouin zone (SBZ) and the high-symmetry $k$ points are shown in Fig. 1(c). From the calculated density of states (DOS) [Fig. 3(a)], we can see that the states around the Fermi level are mainly contributed by Te $p$ orbitals and Ta $d$ orbitals, while Ir $d$ orbitals have relatively small contributions. The common peaks among these states indicate strong $p$-$d$ hybridization in monolayer $TaIrTe_4$.

The band structure of monolayer $TaIrTe_4$ along the high-symmetry paths of SBZ calculated without spin-orbit coupling (SOC) and with SOC are shown in Figs. 3(b) and 3(c), respectively. Without SOC, monolayer $TaIrTe_4$ is a Dirac semimetal, which has a band crossing along the $S$-$Y$ path and a band inversion around the $Y$ point [Fig. 3(b)]. Moreover, the bands around the Fermi level have small dispersion along the $\Gamma$-$Y$ path, which is vertical to the atomic chain direction ($a$ axis) in real space [Fig. 1(b)]. We have also examined the band structure by using the hybrid functional with the HSE06 version [30], which gives similar results. When including SOC, notable changes take place in the band structure. Monolayer $TaIrTe_4$ transforms to an insulator with a band gap of 32 meV. Meanwhile we also calculated the topological invariant $Z_2$ by using the Wilson loops method [31] and obtained the topological invariant $Z_2$ as 1. This demonstrates that monolayer $TaIrTe_4$ is a quantum spin Hall insulator [15,16], similar to monolayer $WTe_2$ [9].

According to the bulk-boundary correspondence, the nontrivial topological property of bulk accompanies the nontrivial edge or surface states at its boundaries. The edge states of monolayer $TaIrTe_4$ were calculated in the open boundary condition. Both the left and right terminated edges of monolayer $TaIrTe_4$ along the $b$ axis are made up of Ta, Ir, and Te atoms [Figs. 1(a) and 1(b)]. As a result, the edge states at the left and

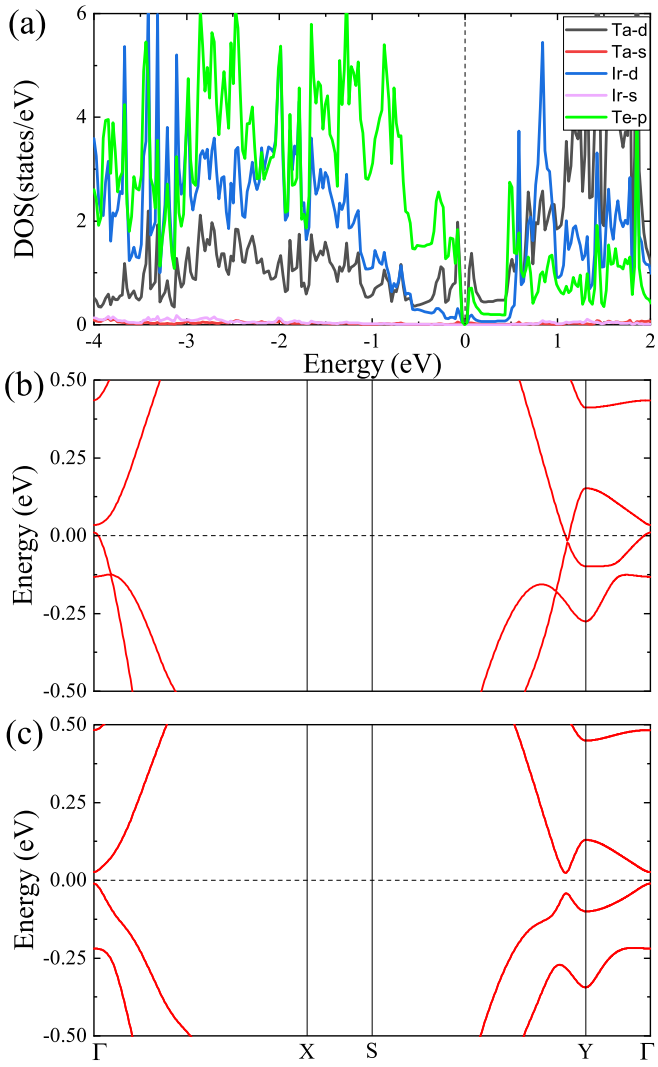


FIG. 3. Electronic structure of monolayer $TaIrTe_4$: (a) density of states; band structures calculated (b) without and (c) with spin-orbit coupling.

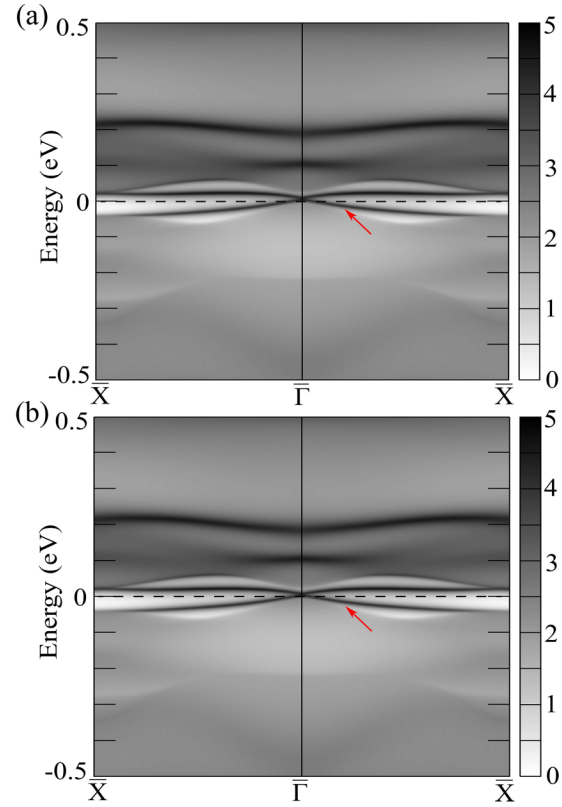


FIG. 4. Spectral function of monolayer $TaIrTe_4$ with a semi-infinite termination edge. The corresponding edge states are highlighted by red arrows. The white-black color scale represents the spectral density with the unit of states per eV.

right terminations along the $b$ axis are very similar [Figs. 4(a) and 4(b)] even though the two terminations are in difference with a fractional translation [Fig. 1(b)]. Meanwhile, the Dirac cone located at the $\overline{\Gamma}$ point is very close to the Fermi level.

In comparison with monolayer $TaIrTe_4$, the space inversion symmetry is absent in bilayer $TaIrTe_4$. Bilayer $TaIrTe_4$ has the $P1m1$ symmorphic space group symmetry. The corresponding point-group symmetry operations contain invariant $E$ and mirror reflection $M_x$. Figure 5 shows the calculated band structure of bilayer $TaIrTe_4$. The bilayer appears to be a Weyl semimetal without including SOC, as shown in Fig. 5(a), in which there is a band crossing along the $\Gamma$-$X$ path as well as band inversion around the $\Gamma$ point of the SBZ. With the inclusion of SOC, the spin degeneracy is lifted due to breaking space inversion symmetry. The antisymmetric SOC is so strong that it results in a large band splitting [Fig. 5(b)]. Meanwhile, the band crossing along the $\Gamma$-$X$ path opens an 8-meV gap [inset in Fig. 5(b)]. Remarkably, the calculated topological invariant $Z_2$ is equal to 1, indicating that bilayer $TaIrTe_4$ is still a QSH insulator. We have also examined the band structure by using the SCAN functional [32], which gives similar results.

We further calculated the edge states of bilayer $TaIrTe_4$ with the open boundary condition. The calculated helical edge states of left and right terminations along the $b$ axis are shown in Figs. 6(a) and 6(b), respectively. On this occasion, the two edge states show a difference. The Dirac cone overlaps with the bulk states at the left edge, but not at the right edge. In addition, the Dirac cone of helical edge states for bilayer $TaIrTe_4$ is located at the $\overline{X}$ point, instead of the $\overline{\Gamma}$ point in monolayer $TaIrTe_4$ (Fig. 4).

Although stacking of two QSH insulators is usually considered to give rise to a trivial insulator, once there appear new band inversions, this may, again, make the bilayer nontrival. The calculations show that there are two bands near the Fermi level inverting once around the $\Gamma$ point [Fig. 5(b)], this makes bilayer $TaIrTe_4$ still a QSH insulator. The underlying reason is as follows. In many layered materials, strong interlayer wave-function overlap of $p$ orbitals does occur, known as covalentlike quasibonding (CLQB), which is a result of balanced dispersion attraction and, mostly, Pauli repulsion. The formation of CLQB induces broadening of valence and conduction bands and thus shows layer-dependent band gaps and other electronic structure related properties [18,33–35]. Previously, both elemental layers and compounds of tellurium were found to possess such covalentlike interlayer interaction [17,18]. For bilayer $TaIrTe_4$, the left inset of Fig. 7(a) depicts

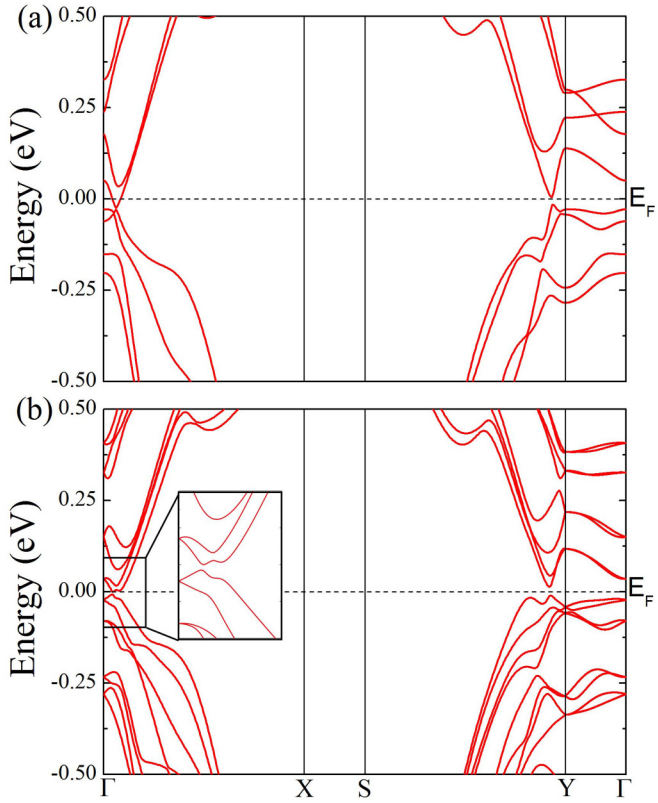


FIG. 5. Band structures of bilayer $TaIrTe_4$ calculated (a) without and (b) with SOC. Inset shows the enlarged band structure around the Γ point.

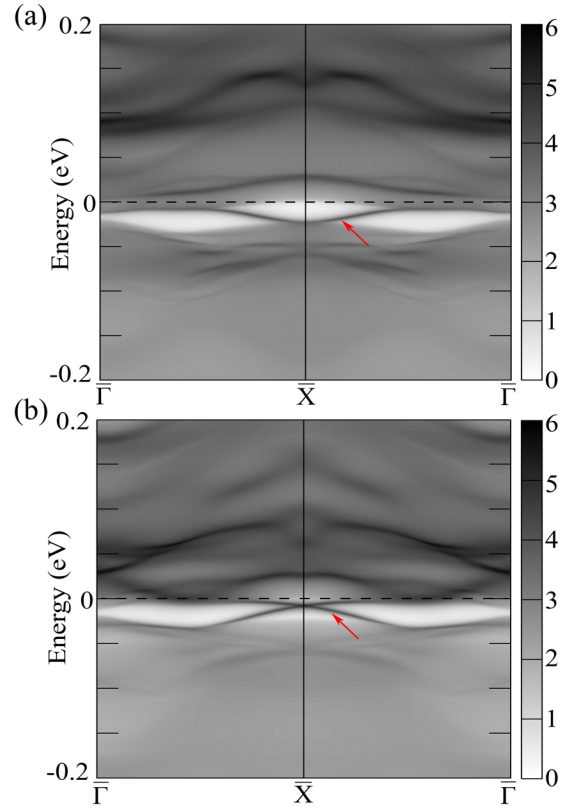


FIG. 6. Spectral function of bilayer $TaIrTe_4$ left (a) and right (b) terminations. Refer to Fig. 1(b) for the definition of left and right terminations. The corresponding edge states are highlighted by red arrows. The white-black color scale represents the spectral density with the unit of states per eV.

a plot of interlayer differential charge densities (DCD) at the equilibrium interlayer distance $d_0$, which explicitly shows charge accumulation (covalent characteristic) at the interlayer region. As shown in Fig. 3, the band gap of monolayer $TaIrTe_4$ is small around the Γ point. Thus the largely broadened valence and conduction bands of bilayer $TaIrTe_4$ give rise to a band inversion over the small band gap around the Γ point [Fig. 5(b)]. In contrast, monolayer $WTe_2$ is a QSH insulator [9] as well as with the covalentlike interlayer bonding, but it possesses large band gaps at the time-reversal invariant points. As a result, bilayer $WTe_2$ is a trivial insulator, as verified by the calculations. Thus the QSH phase is a distinct property of bilayer $TaIrTe_4$.

The interlayer wave-function overlap should gradually weaken as the interlayer distance $d$ increases. Therefore the bilayer will undergo a topological phase transition with the increasing interlayer distance. This analysis is confirmed by our calculation that topological invariant $Z_2$ of the bilayer goes from 1 to 0 in between $d - d_0 = 0.5$ and 1 Å (Fig. 7), indicating a topological nontrivial to trivial transition. While the interlayer charge sharing is clearly shown in DCD plots at distances near $d_0$, no appreciable charge sharing is observable at an interlayer distance $d - d_0 = 2$ Å [Fig. 7(b)], suggesting the CLQB is eliminated.

*Discussion*. As analyzed above, the covalentlike interlayer interaction and the small band gap at the time-reversal invariant point are key factors for the emergence of the QSH phase in bilayer $TaIrTe_4$. Considering that the covalentlike interlayer interaction exists quite popularly in real layered materials, our study suggests that other bilayers or vdW heterostructrues may also realize interesting topological phases, for example, Dirac, Weyl, and node-line semimetals, besides QSH insulators.

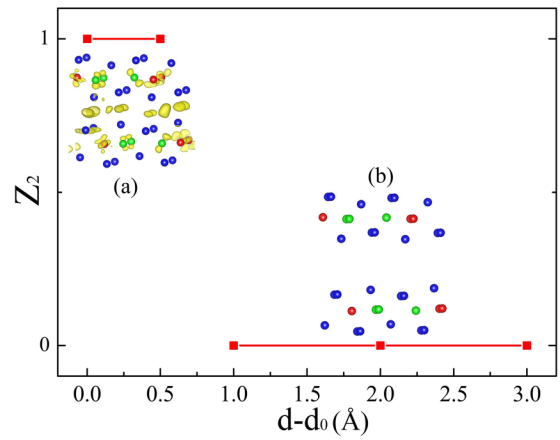


FIG. 7. Topological invariant $Z_2$ with increasing interlayer distance for bilayer $TaIrTe_4$. Differential charge densities for (a) equilibrium structure ($d = d_0$) and (b) enlarged interlayer distance ($d = d_0 + 2$ Å), respectively. Here only positive differential charge densities are illustrated.

A very recent transport experiment found that bulk $TaIrTe_4$ becomes superconducting under pressure [36]. Similarly, the superconductivity in bulk $WTe_2$ [37,38] can be induced by pressure, while the transition from 2D topological insulator to superconductor is driven in monolayer $WTe_2$ via the application of gate voltage [39]. Nontrivial topological superconductivity in monolayer and bilayer $TaIrTe_4$ may also be induced by gate voltage or stress. Furthermore, due to the broken inversion symmetry, Ising superconductivity [40] may be realized in bilayer $TaIrTe_4$.

*Summary*. Based on first-principles electronic structure calculations, we confirm that monolayer $TaIrTe_4$ is a QSH insulator. The Dirac cone of its robust helical edge states located at the $\overline{\Gamma}$ point is very close to the Fermi level. Remarkably, due to the covalentlike interlayer interaction and the small band gap at the time-reversal invariant $\Gamma$ point, bilayer $TaIrTe_4$ is still a QSH insulator. Meanwhile, a topological phase transition is observed by increasing the interlayer distance in bilayer $TaIrTe_4$.

*Acknowledgments.* This work was supported by the National Key R&D Program of China (Grants No. 2017YFA0302903 and No. 2018YFE0202700), the National Natural Science Foundation of China (Grants No. 11774422, No. 11774424, No. 11622437, and No. 11974422), the Strategic Priority Research Program [Chinese Academy of Sciences (CAS)] (Grant No. XDB30000000), the CAS Interdisciplinary Innovation Team, the Fundamental Research Funds for the Central Universities, and the Research Funds of Renmin University of China (Grants No. 16XNLQ01, No. 19XNLG13, and No. 19XNQ025). Computational resources have been provided by the Physical Laboratory of High Performance Computing at Renmin University of China.

[1] M. Z. Hasan and C. L. Kane, Rev. Mod. Phys. **82**, 3045 (2010).
[2] X. L. Qi and S. C. Zhang, Rev. Mod. Phys. **83**, 1057 (2011).
[3] Z. Liu, C. X. Liu, Y. S. Wu, W. H. Duan, F. Liu, and J. Wu, Phys. Rev. Lett. **107**, 136805 (2011).
[4] D. C. Wang, L. Chen, H. M. Liu, and X. L. Wang, J. Phys. Soc. Jpn. **82**, 094712 (2013).
[5] L. Miao, M. Y. Yao, W. M. Ming, F. F. Zhu, C. Q. Han, Z. F. Wang, D. D. Guan, C. L. Gao, C. H. Liu, F. Liu, D. Qian, and J. F. Jia, Phys. Rev. B **91**, 205414 (2015).
[6] L. Peng, J. J. Xian, P. Z. Tang, A. Rubio, S. C. Zhang, W. H. Zhang, and Y. S. Fu, Phys. Rev. B **98**, 245108 (2018).
[7] B. Huang, G. Clark, N. M. Efrén, D. R. Klein, R. Cheng, K. L. Seyler, D. Zhong, E. Schmidgall, M. A. McGuire, H. C. David, W. Yao, D. Xiao, J. H. Pablo, and X. D. Xu, Nature (London) **546**, 270 (2017).
[8] A. A. Soluyanov, D. Gresch, Z. J. Wang, Q. S. Wu, M. Troyer, X. Dai, and B. A. Bernevig, Nature (London) **527**, 495 (2015).
[9] X. F. Qian, J. W. Liu, L. Fu, and J. Li, Science **346**, 1344 (2014).
[10] K. Koepernik, D. Kasinathan, D. V. Efremov, S. Khim, S. Borisenko, B. Büchner, and J. van den Brink, Phys. Rev. B **93**, 201101(R) (2016).
[11] S. Khim, K. Koepernik, D. V. Efremov, J. Klotz, T. Förster, J. Wosnitza, M. I. Sturza, S. Wurmehl, C. Hess, J. van den Brink, and B. Büchner, Phys. Rev. B **94**, 165145 (2016).
[12] I. Belopolski, P. Yu, D. S. Sanchez, Y. Ishida, T. R. Chang, S. T. S. Zhang, S. Y. Xu, H. Zheng, G. Q. Chang, G. Bian, H. T. Jeng, T. Kondo, H. Lin, Z. Liu, S. Shin, and M. Z. Hasan, Nat. Commun. **8**, 942 (2017).
[13] E. Haubold, K. Koepernik, D. Efremov, S. Khim, A. Fedorov, Y. Kushnirenko, J. van den Brink, S. Wurmehl, B. Büchner, T. K. Kim, M. Hoesch, K. Sumida, K. Taguchi, T. Yoshikawa, A. Kimura, T. Okuda, and S. V. Borisenko, Phys. Rev. B **95**, 241108(R) (2017).
[14] X. Q. Zhou, Q. H. Liu, Q. S. Wu, T. Nummy, H. X. Li, J. Griffith, S. Parham, J. Waugh, E. Emmanouilidou, B. Shen, O. V. Yazyev, N. Ni, and D. Dessau, Phys. Rev. B **97**, 241102(R) (2018).
[15] J. W. Liu, H. Wang, C. Fang, L. Fu, and X. F. Qian, Nano Lett. **17**, 467 (2017).
[16] X. Dong, M. Y. Wang, D. Y. Yan, X. L. Peng, J. Li, W. D. Xiao, Q. S. Wang, J. F. Han, J. Ma, Y. G. Shi, and Y. G. Yao, ACS Nano **13**, 9571 (2019).
[17] C. Liu, C. S. Lian, M. H. Liao, Y. Wang, Y. Zhong, C. Ding, W. Li, C. L. Song, K. He, X. C. Ma, W. H. Duan, D. Zhang, Y. Xu, L. L. Wang, and Q. K. Xue, Phys. Rev. Mater. **2**, 094001 (2018).
[18] J. S. Qiao, Y. H. Pan, F. Yang, C. Wang, Y. Chai, and W. Ji, Sci. Bull. **63**, 159 (2018).
[19] P. E. Blöchl, Phys. Rev. B **50**, 17953 (1994).
[20] G. Kresse and D. Joubert, Phys. Rev. B **59**, 1758 (1999).
[21] G. Kresse and J. Hafner, Phys. Rev. B **47**, 558 (1993).
[22] G. Kresse and J. Furthmüller, Comput. Mater. Sci. **6**, 15 (1996).
[23] G. Kresse and J. Furthmüller, Phys. Rev. B **54**, 11169 (1996).
[24] J. P. Perdew, K. Burke, and M. Ernzerhof, Phys. Rev. Lett. **77**, 3865 (1996).
[25] J. Klimeš, D. R. Bowler, and A. Michaelides, Phys. Rev. B **83**, 195131 (2011).
[26] A. Mar, S. Jobic, and J. A. Ibers, J. Am. Chem. Soc. **114**, 8963 (1992).
[27] Q. S. Wu, S. Zhang, H. F. Song, M. Troyer, and A. A. Soluyanov, Comput. Phys. Commun. **224**, 405 (2018).
[28] R. Zacharia, H. Ulbricht, and T. Hertel, Phys. Rev. B **69**, 155406 (2004).
[29] Y. N. Liu, Q. Q. Gu, Y. Peng, S. M. Qi, N. Zhang, Y. N. Zhang, X. M. Ma, R. Zhu, L. M. Tong, J. Feng, Z. Liu, and J. H. Chen, Adv. Mater. **30**, 1706402 (2018).
[30] A. V. Krukau, O. A. Vydrov, A. F. Izmaylov, and G. E. Scuseria, J. Chem. Phys. **125**, 224106 (2006).
[31] R. Yu, X. L. Qi, A. Bernevig, Z. Fang, and X. Dai, Phys. Rev. B **84**, 075119 (2011).
[32] J. W. Sun, A. Ruzsinszky, and J. P. Perdew, Phys. Rev. Lett. **115**, 036402 (2015).
[33] J. S. Qiao, X. Kong, Z. X. Hu, F. Yang, and W. Ji, Nat. Commun. **5**, 4475 (2014).
[34] Y. D. Zhao, J. S. Qiao, Z. H. Yu, P. Yu, K. Xu, S. P. Lau, W. Zhou, Z. Liu, X. R. Wang, W. Ji, and Y. Chai, Adv. Mater. **29**, 1604230 (2016).

[35] C. Wang, X. Y. Zhou, Y. H. Pan, J. S. Qiao, X. H. Kong, C. C. Kaun, and W. Ji, Phys Rev B **97**, 245409 (2018).

[36] S. Cai, E. Emmanouilidou, J. Guo, X. D. Li, Y. C. Li, K. Yang, A. Li, Q. Wu, N. Ni, and L. L. Sun, Phys. Rev. B **99**, 020503(R) (2019).

[37] D. F. Kang, Y. Z. Zhou, W. Yi, C. L. Yang, J. Guo, Y. G. Shi, S. Zhang, Z. Wang, C. Zhang, S. Jiang, A. G. Li, K. Yang, Q. Wu, G. M. Zhang, L. L. Sun, and Z. X. Zhao, Nat. Commun. **6**, 7804 (2015).

[38] X. C. Pan, X. L. Chen, H. M. Liu, Y. Q. Feng, Z. X. Wei, Y. H. Zhou, Z. H. Chi, L. Pi, F. Yen, F. Q. Song, X. G. Wan, Z. R. Yang, B. G. Wang, G. H. Wang, and Y. H. Zhang, Nat. Commun. **6**, 7805 (2015).

[39] E. Sajadi, T. Palomaki, Z. Y. Fei, W. J. Zhao, P. Bement, C. Olsen, S. Luescher, X. D. Xu, J. A. Folk, and D. H. Cobden, Science **362**, 922 (2018).

[40] X. X. Xi, Z. F. Wang, W. W. Zhao, J. H. Park, K. T. Law, H. Berger, L. Forró, J. Shan, and K. F. Mak, Nat. Phys. **12**, 139 (2016).